MAUSAM, **67**, 2 (April 2016), 411-422

551.501.9 : 621.396.969 (512.317)

Calculation and application of eddy dissipation rate map based on spectrum width data of a S-band radar in Hong Kong

P. W. CHAN, P. ZHANG*, R. DOVIAK**

Hong Kong Observatory, Hong Kong, China

** CIMMS, University of Oklahoma, Norman, Oklahoma*

***NOAA/National Severe Storms Laboratory, Norman, Oklahoma*

(*Received 22 July 2014, Accepted 15 December 2014*)

e mail : pwchan@hko.gov.hk

सार – इस शोध पत्र में पर्ल नदी डेल्टा क्षेत्र में वायुयान के मार्ग में विक्षोभ सतर्कता सेवा उपलब्ध कराने के उद्देश्य से बवंडर क्षय दर (EDR) के मानचित्र को आकलित करने के लिए हांग कांग में एस-बैंड रेडार के स्पेक्ट्रम विस्तार के आँकड़ों का उपयोग किया गया। आकलित वर्गीकरण वर्तमान लिटरेचर में बताए गए आकलन से भिन्न है जो रेडार आधारित EDR निर्धारण में पवन अपरूपण को भी दूर करता है। रेडार कोनिकल स्कैन से प्राप्त हुए मानचित्रों के निष्पादन को वायुयान द्वारा बताए जाने वाले सामान्य से प्रचंड विक्षोभ के दो उदाहरणों में दिखाया गया है। वायुयान के आँकड़ों से निर्धारित किए गए EDR मानों और पवन अपरूपण आपदा कारकों के आधार पर दोनों मामलों में वायुप्रवाहित विक्षोभ वायुयान के प्रचालन को प्रतिकूल रूप से प्रभावित कर सकते हैं। रेडार के परावर्तक चित्रों पर उड़ान के मार्ग को अधिचित्रित करने पर यह पता चला है कि दोनों मामलों में विक्षुब्ध वायुप्रवाह तीव्र वर्षा के कोशिकाओं से संबंद्ध थे हालांकि वे अपेक्षाकृत छोटे और अलग-थलग थे। वर्षा कोशिकाओं वाले स्थानों पर रेडार के स्पेक्ट्रम विस्तार आँकड़ों से आकलित किए गए EDR के मान वायुयान से पवन मापों द्वारा निर्धारित मापों के अनुकूल रहें। कुछ चुने हुए मामलों से यह पता चला है कि रेडार आधारित EDR में सामान्यत: गुणवत्ता संतोषजनक रही। आँकड़ों को जोड़ते हुए यदि कॉकपिट पर ऐसे आँकड़े उपलब्ध हो सकेंगे तो पॉयलटों को उपयोगी संकेत मिल सकेंगे कि वे वर्षा कोशिकाओं से नहीं बल्कि उसके आस पास वाले क्षेत्र से उड़ान भरे। पर्ल नदी डेल्टा क्षेत्र के रेडारो में प्रणाली विज्ञान प्रयुक्त की जा सकती है ताकि विमानन सुरक्षा को आश्वस्त करने के लिए विक्षोभ तीव्रता के तीन आयामी मेज़ेइक निर्मित किए जा सकेंगे।

ABSTRACT. The spectrum width data of an S-band radar in Hong Kong are used to calculate the map of eddy dissipation rate (EDR) with the objective of providing turbulence alerting service for the en-route aircraft in the Pearl River Delta region. The calculation methodology is different from that reported in the existing literature by also removing the wind shear contribution in determining the radar-based EDR. The performance of the EDR maps obtained from the conical scans of the radar is illustrated in two examples of moderate to severe turbulence reported by the aircraft. In both cases, based on the EDR values and windshear hazard factors determined from the aircraft data, the airflow disturbances could adversely affect the operation of the aircraft. By overlaying the flight route on the radar's reflectivity imageries, it appears that, in both cases, the disturbed airflow is associated with rather intense rain cells, though they are rather small and isolated. The EDR values calculated from the radar's spectrum width data at the locations of the rain cells are generally consistent with those determined using the aircraft's wind measurements. From the selected cases, it seems that the radar-based EDR values have generally satisfactory quality. If such data could be available at the cockpit through data uplinking, they could be useful hints for the pilots not to fly through the rain cells but rather going around them. The methodology may be applied to the radars in the Pearl River Delta region in order to construct a three-dimensional mosaic of turbulence intensity for the assurance of aviation safety.

Key words – Weather radar, Eddy dissipation rate, Severe turbulence.

1. Introduction

Turbulence could be hazardous to the operation of the aircraft. According to the International Civil Aviation Organization (ICAO, 2010), moderate and severe turbulence need to be reported. In particular, severe turbulence may cause momentary loss of control of the aircraft. The turbulence reporting nowadays is mainly based on the subjective perception of the airflow disturbances by the pilots. The objective definition of

severity of turbulence is based on the cube root of eddy dissipation rate (EDR), as discussed in ICAO (2010). For en-route aircraft, $EDR^{1/3}$ value between 0.4 $m^{2/3}s^{-1}$ and 0.7 $m^{2/3}s^{-1}$ is taken to be moderate turbulence and $EDR^{1/3}$ value exceeding 0.7 $m^{2/3}s^{-1}$ is taken to be severe turbulence.

Besides the measurements made onboard the aircraft, turbulence could be calculated using remote-sensing technology. For instance, Chan (2011) uses the structure function approach to calculate the turbulence map in the vicinity of the Hong Kong International Airport (HKIA) based on the wind measurements from a Doppler Light Detection And Ranging (LIDAR) system, which works best under clear air or non-rainy weather conditions. A LIDAR windshear alerting system has been implemented at HKIA (Shun and Chan, 2008). The LIDAR-derived turbulence intensity map has also been compared with results from numerical weather prediction model (Chan, 2009). On the other hand, in case of rain (*e.g*., in intense convective weather), the data from microwave weather radars may be used. Zhang *et al*. (2009) use the spectrum width data from a C-band radar at HKIA, namely, Terminal Doppler Weather Radar (TDWR) in calculating turbulence map near the airport. The turbulence data so obtained have reasonable correlation with the turbulence intensities as measured on the aircraft in selected cases of rainy weather. TDWR and similar weather radars have been used for monitoring low-level windshear as well, such as Merritt (1987) and Proctor *et al*. (2000). For turbulence, comparison between aircraft and radar observations has been made by Labitt (1981).

There are a number of systems used for alerting turbulence near the airport, such as the one developed for Juneau airport (Gilbert *et al*., 2004) and Hong Kong airport (Clark *et al*., 1997). A summary in the latest development of turbulence alerting algorithm could be found in Cornman *et al*. (2004). The spectrum width data of WSR-88D radar in the US have also been used for turbulence detection purpose (Fang *et al*., 2004).

The above studies mainly focus on low-level turbulence alerting, namely, when the aircraft is within 3 nautical miles away from the runway end or below 1600 feet from the runway surface. There are also attempts to alert the en-route aircraft about the threat of turbulence based on remote-sensing data. For instance, Williams (2006) describe in detail a method called the NEXRAD Turbulence Detection Algorithm (NTDA) to construct the three-dimensional mosaic of $EDR^{1/3}$ over continental US based on the spectrum width data of weather radars. However, in the formulation of NTDA, the wind shear term, which contributes to the spectrum width, is not removed explicitly. This removal is made, though in a rough approximation, in the methodology considered in Zhang (2009) for TDWR. In this paper, similar calculation of $EDR^{1/3}$ based on spectrum width data of a long-range, S-band radar in Hong Kong is made to explore the possibility of alerting the en-route aircraft about the turbulence threat, with the proper removal of wind shear effect.

How to remove wind shear contribution from spectrum width is very important for estimating the intensity of turbulence (EDR), but it is really hard to accurately subtracting the ambient wind shear field. Spatial resolution of radar beam width and its spatial expansion along radial are the major difficulties for accurately calculating the wind shear contribution. The approach in this paper just roughly estimates and removes the wind shear contribution from the spectrum width measurements. The spatial change of the wind shear estimation as radar resolution volume increase with range is not considered in the present method.

After discussion of the methodology, the algorithm is applied to two cases of moderate and severe turbulence in convective rain cells in the vicinity of Hong Kong to demonstrate the usefulness of the calculated EDR. In particular, the EDR so determined is compared with the subjective perception as reported from the pilot and the objective EDR data determined from the flight data, following the method in Haverdings and Chan (2010).

2. Methodology

It has been known that spectrum width measured by Doppler radar can be utilized to estimate atmospheric turbulence intensity. The measurement of spectrum width is determined not only by the Doppler velocity distribution and density distribution of the scatterers within the resolution volume, but also radar observation parameters like beam width, pulse width, antenna rotation rate, etc. According to Doviak and Zrnic (2006), there are five major spectral broadening mechanisms that contribute to the spectrum width measurements, which can be written as follow:

$$\sigma_v^2 = \sigma_s^2 + \sigma_t^2 + \sigma_\alpha^2 + \sigma_d^2 + \sigma_o^2 \qquad (1)$$

where, σ_s represents mean wind shear contribution, σ_t represents turbulence, σ_α represents antenna motion, σ_d represents different terminal velocities of hydrometeors of different sizes and σ_o represents variations of orientations and vibrations of hydrometeors. Except σ_s and σ_t, the rest of the terms on the right hand side of the Eqn. (1) are considered to be negligible for the measurements of σ_v in our scheme (Brewster and Zrnic, 1986). Thus, turbulence

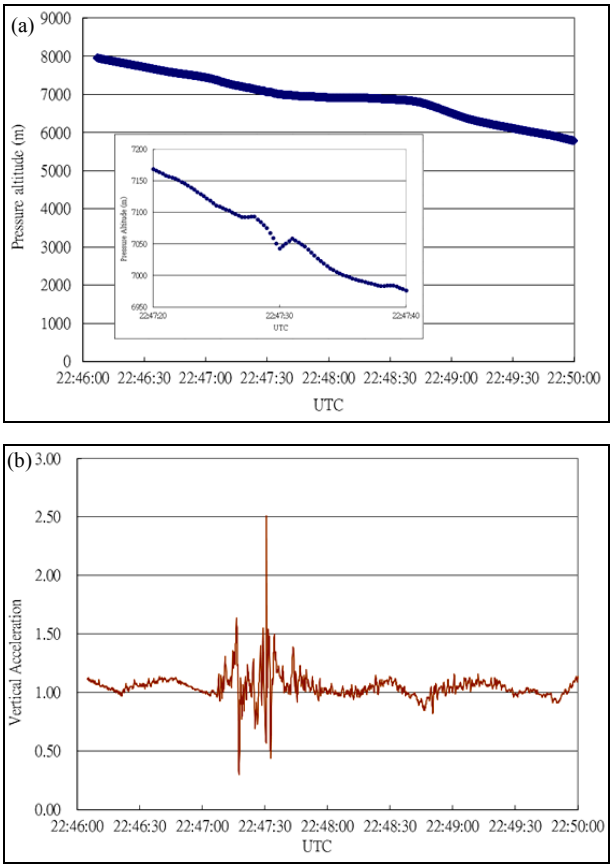

Figs. 1(a&b). (a) The altitude of the aircraft and (b) the vertical acceleration measured on the aircraft for the first turbulence case. A zoom-in of the altitude when the g variation is large is given in the inset of (a)

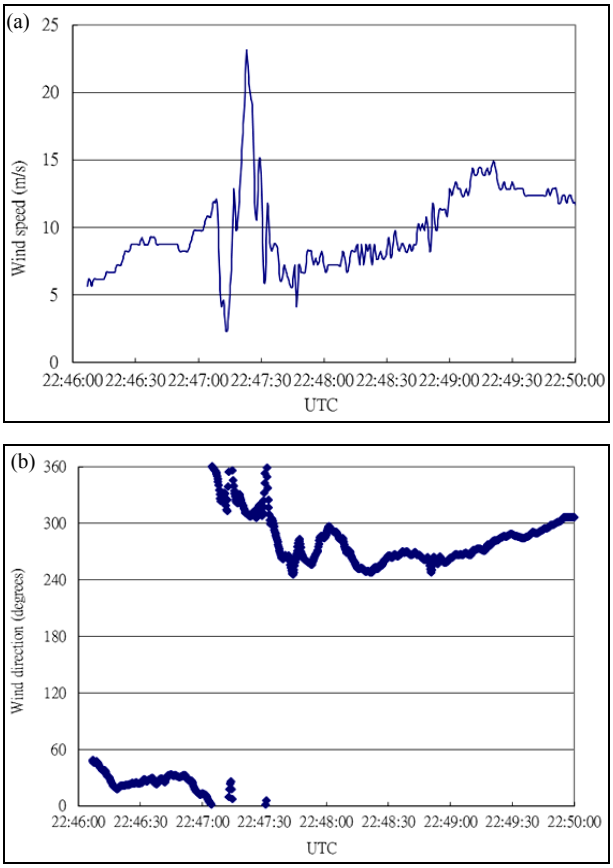

Figs. 2(a&b). (a)Wind speed and (b) wind direction (b) measured onboard the aircraft for the first turbulence case

contribution σ_s to the measured spectrum width σ_v can be obtained by subtracting mean wind shear contribution σ_s,

$$\sigma_t^2 = \sigma_v^2 - \sigma_s^2 \quad (2)$$

In the Eqn. (2), mean wind shear width term σ_s can be decomposed into three terms due to mean radial velocity shear at three orthogonal directions in radar coordinate (Doviak and Zrnic, 2006):

$$\sigma_s^2 = \sigma_{s\theta}^2 + \sigma_{s\phi}^2 + \sigma_{sr}^2 = (r_0\sigma_\theta k_\theta)^2 + (r_0\sigma_\phi k_\phi)^2 + (\sigma_r k_r)^2 \quad (3)$$

where $\sigma_r^2 = (0.35c\tau/2)^2$, $\sigma_\theta^2 = \theta_1^2/16\ln 2$ and $\sigma_\phi^2 = \theta_1^2/16\ln 2$. Here $c\tau/2$ is range resolution, and θ_1 is the one-way angular resolution (*i.e.*, beamwidth). k_θ, k_ϕ and k_r are the components of shear along the three orthogonal directions, c is speed of light in a vacuum, τ is pulse width, r_o is the distance between radar and the center of resolution volume. K_θ is wind shear in θ (elevation) direction; K_ϕ is wind shear in ϕ (azimuthal) direction; and K_r is wind shear in r direction (range).

EDR ε can be estimated by using σ_t. Under these assumptions, the relation between turbulence spectrum width σ_t and EDR ε can be approximately written as:

$$\varepsilon \approx \left[\frac{<\sigma_t^2>^{3/2}}{\sigma_r (1.35A)^{3/2}}\right]\left(\frac{11}{15} + \frac{4}{15}\frac{r^2\sigma_\theta^2}{\sigma_r^2}\right)^{-3/2} \quad (4)$$

A is a non-dimensional constant with a value of 1.6.

The Eqn. (4) is used to estimate EDR using Hong Kong S band radar observed spectrum width. The mean radial velocity shears at the radar gate at three orthogonal directions are calculated and subtracted from observed spectrum width.

The radar under consideration in this paper is located at Tai Mo Shan, the highest mountain in Hong Kong, with a height of about 970 m above mean sea level. The radar

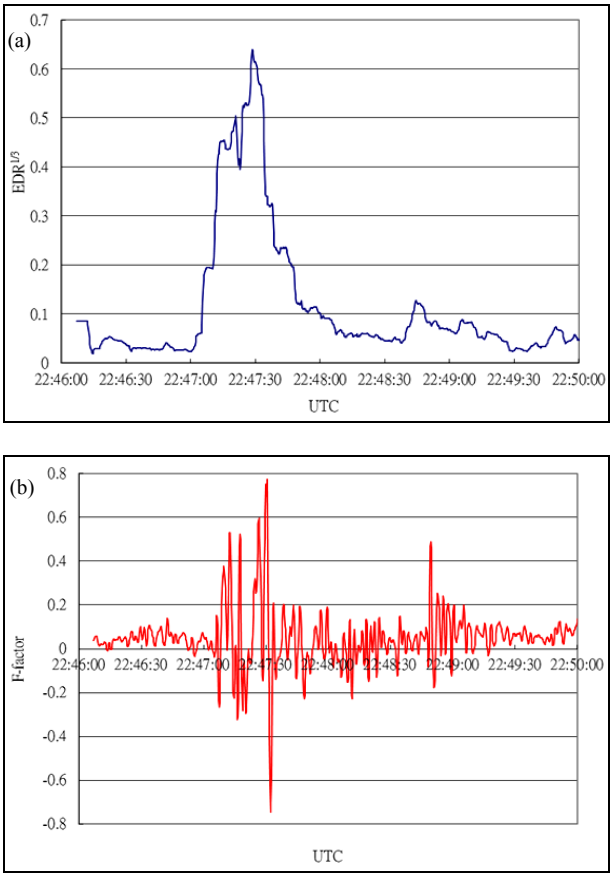

Figs. 3(a&b). The time series of (a) $EDR^{1/3}$ and (b) F-factor of the aircraft in the first turbulence case

antenna beam width is 0.9 degrees and the transmitter frequency is 2.82 GHz. Klystron transmitter is used. The radar makes a volume scan every 6 minutes with the elevation angles of 0.0, 0.9, 1.8, 2.7, 3.6, 5.4, 10.0, 15.0, 22.0 and 34.0 degrees. It also makes a long-range surveillance scan at an elevation range of 0.0 degrees. The spectrum width data obtained in the volume scan are considered in this paper in the calculation of EDR map. The data in the conical scans are used directly without interpolation to a three-dimensional Cartesian grid.

3. First example – Moderate to severe turbulence on 12 August, 2009

According to the pilot report for this case, on descent passing flight level (FL) 250 (*i.e.*, a height of about 25,000 feet above sea level) heading approximately south, the aircraft encountered moderate to severe turbulence. The aircraft passed the edge of a cumulonimbus (CB) as it was turning to avoid many CBs. The cabin crews were instructed to be seated. All passengers were already seated. Seatbelt signs were on and thus there was no injury for this case.

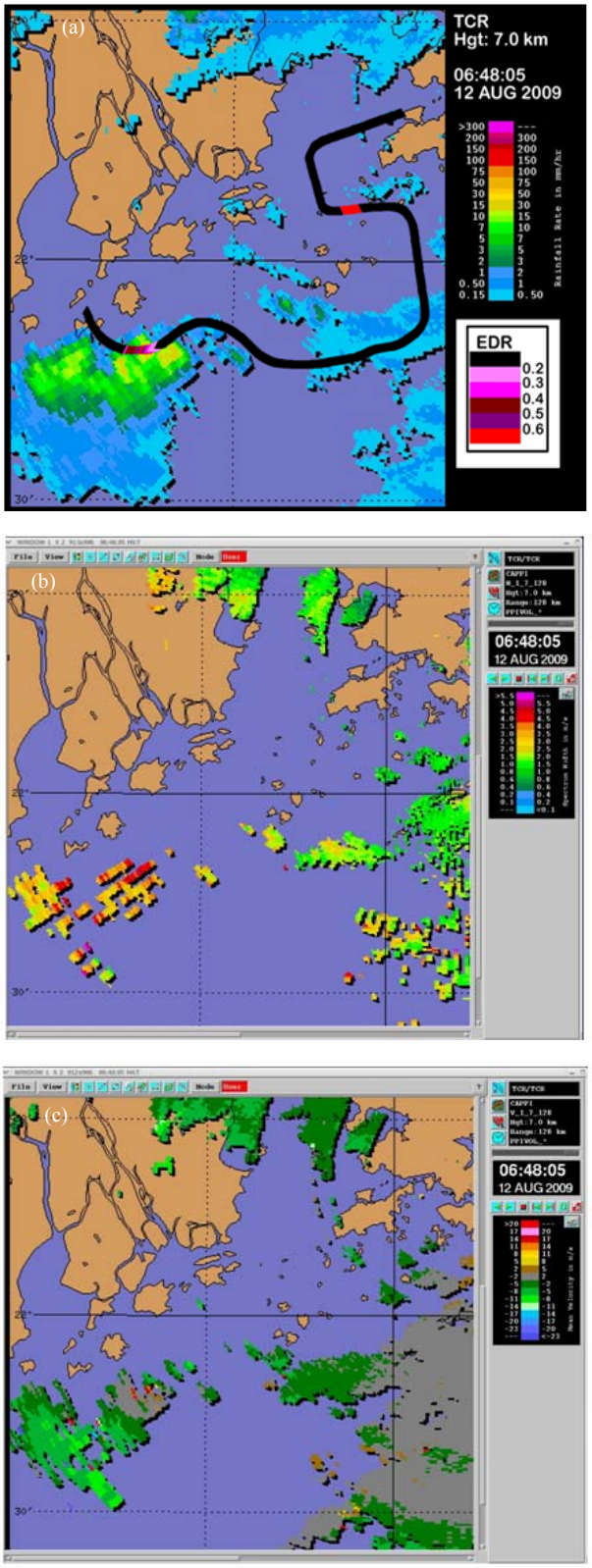

Figs. 4(a-c). The radar reflectivity overlaid with (a) the available $EDR^{1/3}$ data from the aircraft, (b) the radar's spectrum width and (c) its Doppler velocity at a height of 7000 m for the first turbulence case.

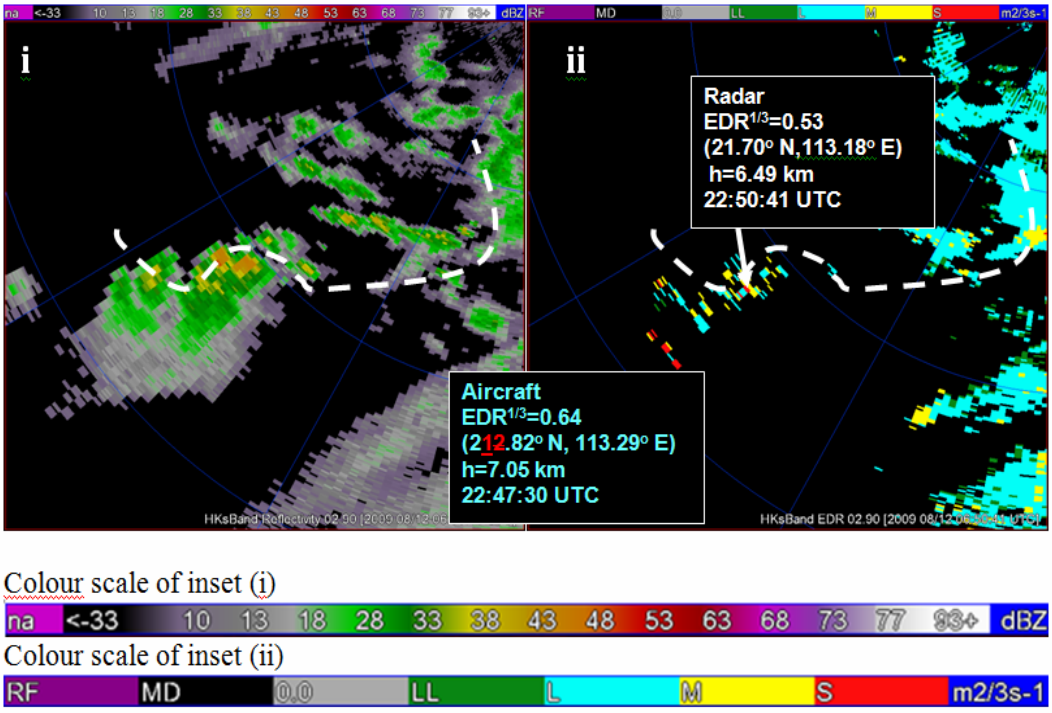

Fig. 5(a). (i) Reflectivity and (ii) $EDR^{1/3}$ fields at elevation angle of 2.9° at 22:50 UTC on 11 August, 2009. White dash line indicates the flight path. Please note that, in (ii), the colour-scale of $EDR^{1/3}$ for low-level turbulence is used, namely, L (light) means 0.1 to 0.3, M (moderate) means 0.3 to 0.5, and S (severe) means above 0.5 (unit : $m^2/3s^{-1}$)

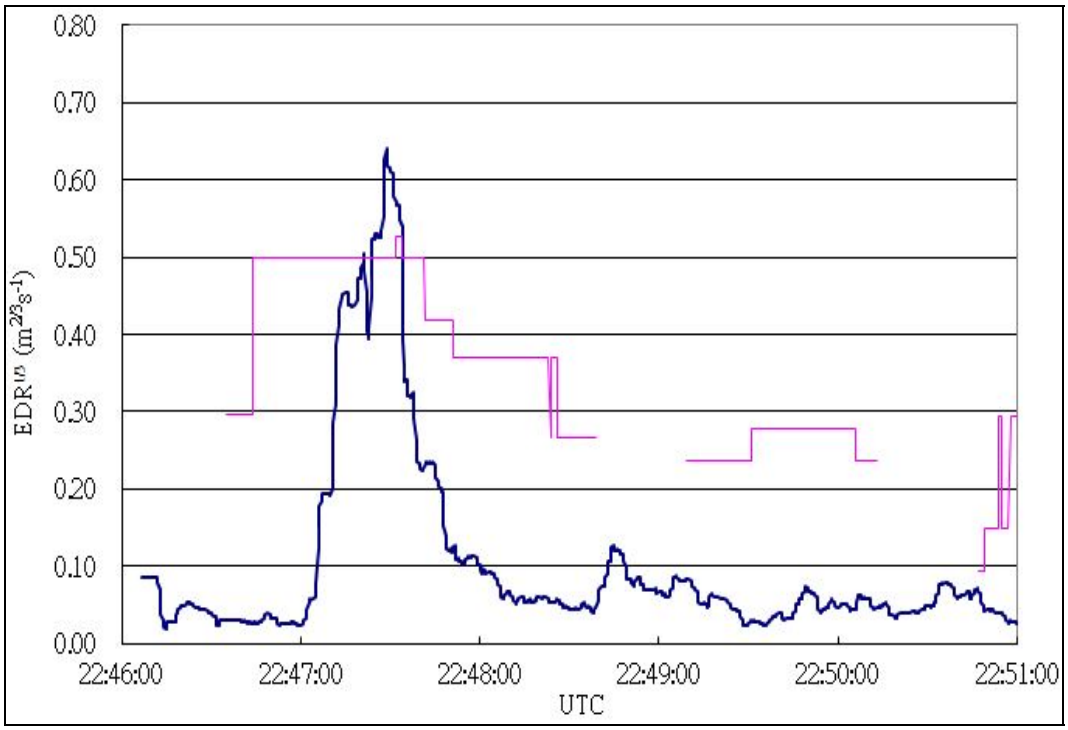

Fig. 5(b). Time series graph for comparing $EDR^{1/3}$ between aircraft (blue) and radar (pink) on 11th August, 2009 over Hong Kong International airport

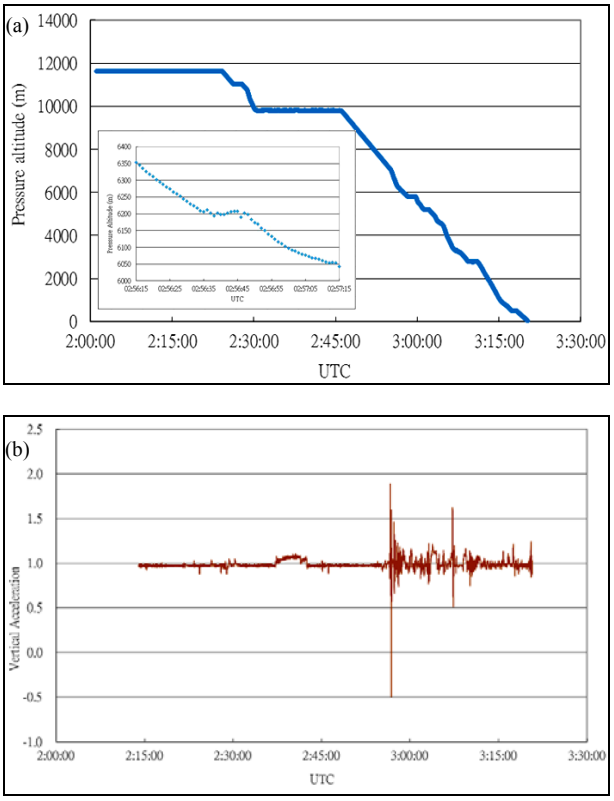

Figs. 6(a&b). (a) Altitude of the aircraft and (b) vertical acceleration measured on the aircraft on 13th May 2011 over Hong Kong International airport. A zoom-in of the altitude when the g variation is large is given in the inset of (a)

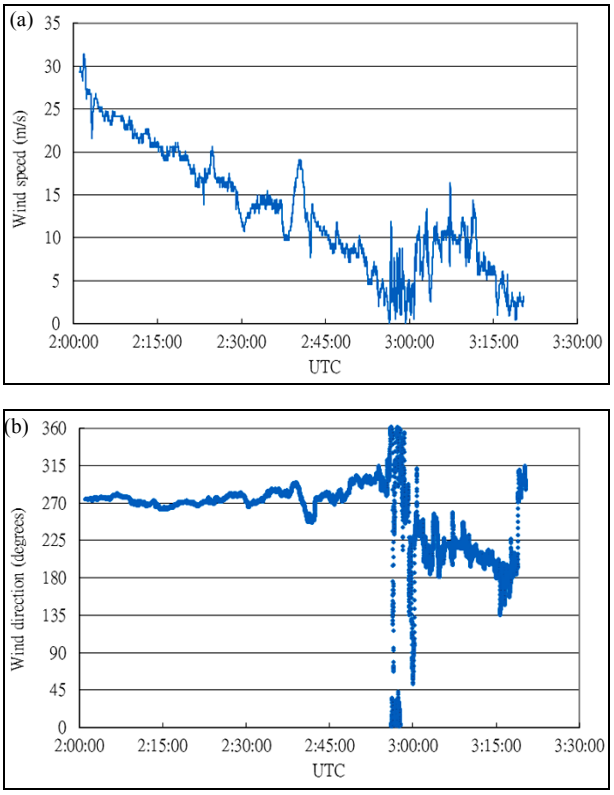

Figs. 7(a&b). (a) Wind speed and (b) wind direction measured onboard the aircraft for the second turbulence case

Based on the aircraft data, the moderate to severe turbulence event took place at about 22:47:30 UTC, 11 August (which is 06:47:30 Hong Kong time [HKT], 12 August, with HKT = UTC + 8 hours). At that time, the aircraft had an altitude of about 7000 m above sea level [Fig. 1(a)]. The vertical acceleration fluctuated rather rapidly between 22:47:10 and 22:47:40 UTC, reaching a maximum of 2.5 g at the peak of the event [22:47:30 UTC, Fig. 1(b)]. The winds were mainly north northwesterly in the above period [Fig. 2(b)]. They once reached a maximum of about 24 m/s shortly before the peak of the event [Fig. 2(a)] and decreased gradually to about 4 m/s afterwards.

Synoptically, in the morning of 12 August, 2009, a surface trough of low pressure was bringing unsettled weather to the south China coastal areas. Mesoscale cyclonic circulations could be analyzed along the coast in the lower and middle troposphere. The strong to gale northerly winds at 7000 m above sea level could be associated with the western flank of a cyclonic circulation.

The impact of the event on the operation of the aircraft could be seen from the time series plots of EDR and the windshear hazard factor, or F-factor (Hinton, 1993). The plot of the cube root of EDR is given in Fig. 3(a). It could be seen that the maximum value of $EDR^{1/3}$ lies between 0.4 and 0.7 $m^{2/3}s^{-1}$. Thus the $EDR^{1/3}$ value also supports that the event is moderate turbulence, close to severe turbulence. The F-factor [Fig. 3(b)] reaches a maximum magnitude of about 0.8 (both positive and negative), which far exceeds the alerting level of 0.105 (Hinton, 1993). As such, the event has significant effect on the operation of the aircraft in terms of turbulence and windshear.

The calculated $EDR^{1/3}$ values from the available flight data are overlaid on the reflectivity imagery at a height of about 7 km above sea level from the S-band radar at Tai Mo Shan, as shown in Fig. 4(a). It could be seen that the moderate to severe turbulence event occurred inside a rain cell with an estimated rainfall rate of 50-75 mm/hour (coloured yellow to orange) when the aircraft was located at about 90 km to the southwest of HKIA. Based on the aircraft data and the radar observations, the moderate to severe event may be related to the aircraft flying an isolated but rather intense rain cell.

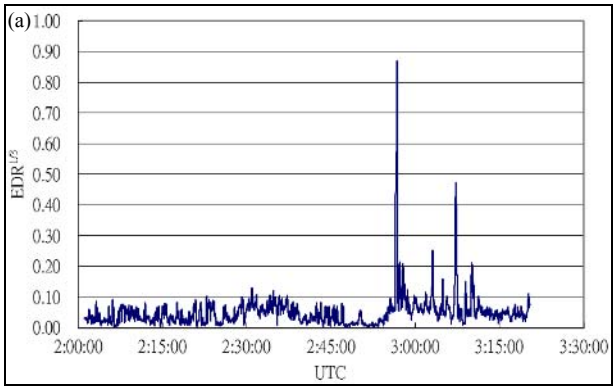

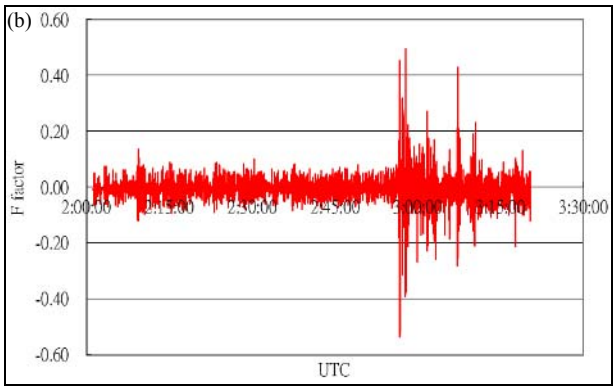

Figs. 8(a&b). The time series of (a) $EDR^{1/3}$ and (b) F-factor of the aircraft in the second turbulence case

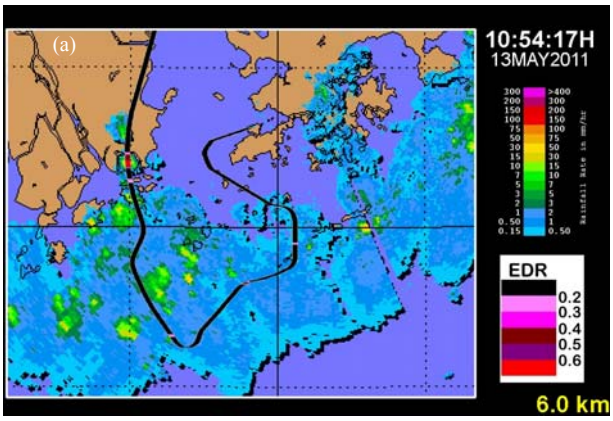

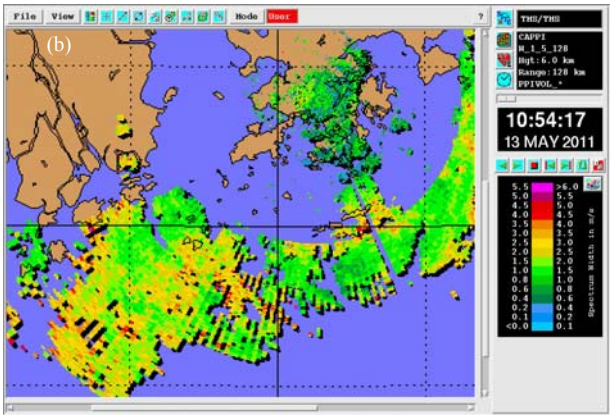

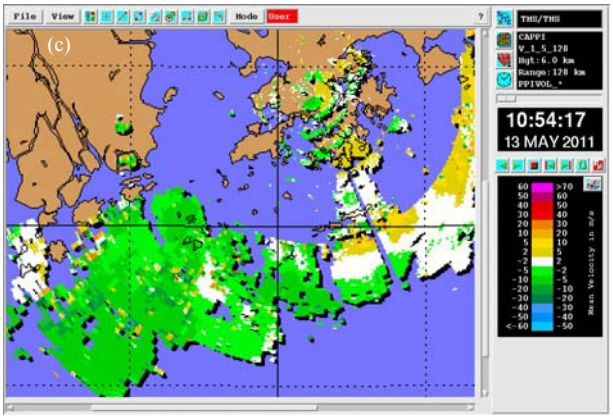

Figs. 9(a-c). The radar reflectivity overlaid with the (a) available $EDR^{1/3}$ data from the aircraft , (b) the radar's spectrum width and (c) its Doppler velocity at a height of 6000 m for the second turbulence case

From the radar measurements, the spectrum width at the location of the event appears to be quite high [Fig. 4(b)], reaching a maximum value in the region of about 4 m/s. The radial velocity, on the other hand, seems to be rather low. In Fig. 4(c), the Doppler velocity measured by the radar at the height of the event is mainly in the region of 2 to 5 m/s only but for a few isolated high velocity of the order 14 m/s. The relatively small value of Doppler velocity may be related to the fact that the northwesterly wind is basically perpendicular to the line-of-sight direction of the radar at the location of the event.

The EDR value estimated from the spectrum width is compared with that obtained from the aircraft data. At the peak of the event, the $EDR^{1/3}$ reached about 0.6 $m^{2/3}s^{-1}$. The $EDR^{1/3}$ estimated from the spectrum width of the radar at the location of the intense rain cell could get to about 0.53 $m^{2/3}s^{-1}$ [Fig. 5(a)], located at about 10 km from the aircraft's flight route. Both datasets indicate that the event is related to moderate to severe turbulence. If the radar-based $EDR^{1/3}$ value could be provided to the aircraft in real-time, it would help the pilot set that, though the rain cell appeared to be rather small, the turbulence level inside the cell may get to rather high value and thus it would be advisable to fly around the cell instead of going straight into it. New uplink technology such as electronic flight bag (EFB), which allows uplinking of the

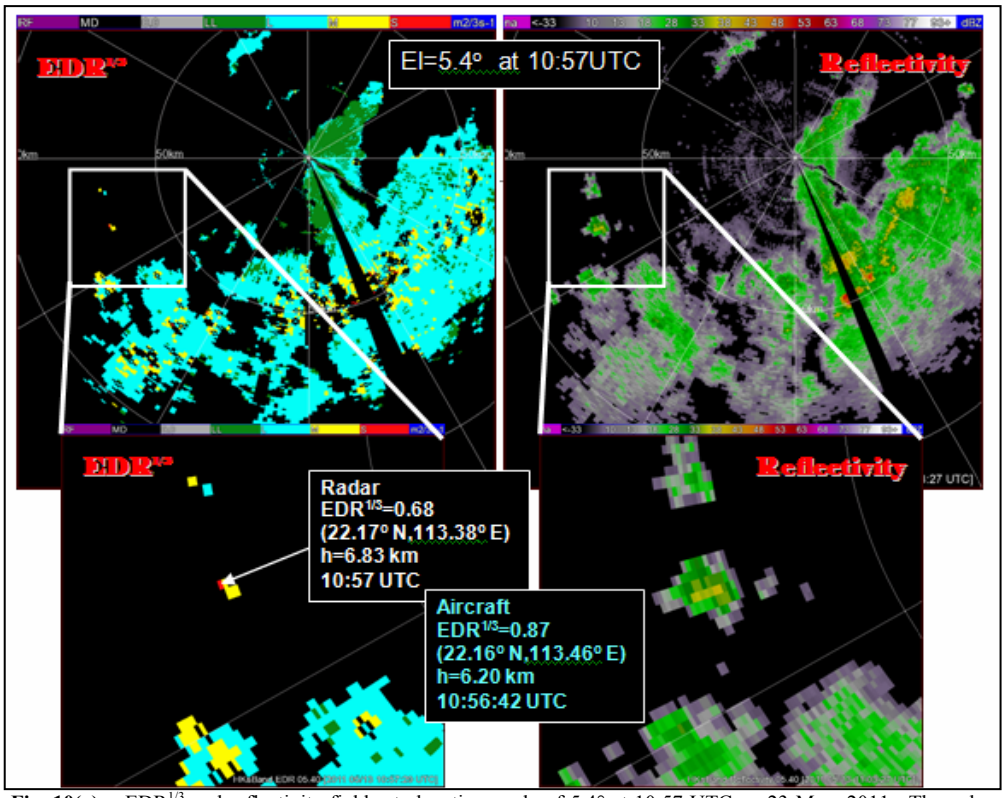

Fig. 10(a). $EDR^{1/3}$ and reflectivity fields at elevation angle of 5.4° at 10:57 UTC on 23 May, 2011. The colour scale of left hand side is the same as that of Fig. 5(a)(ii)

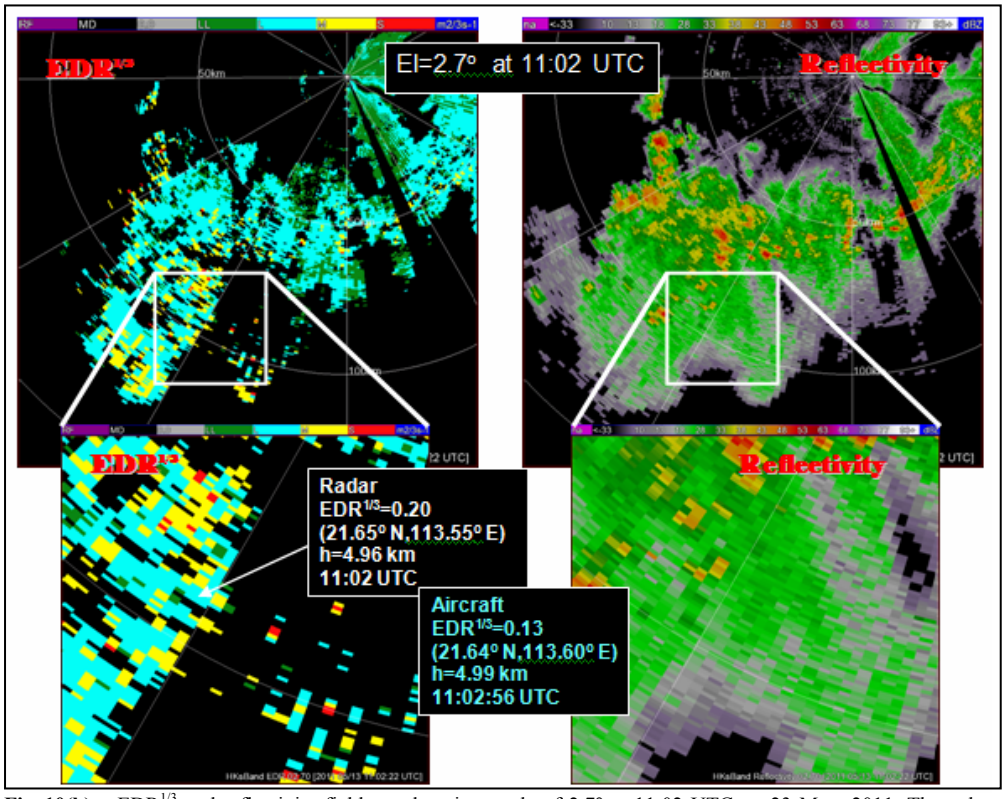

Fig. 10(b). $EDR^{1/3}$ and reflectivity fields at elevation angle of 2.7° at 11:02 UTC on 23 May, 2011. The colour scale of left hand side is the same as that of Fig. 5(a)(ii)

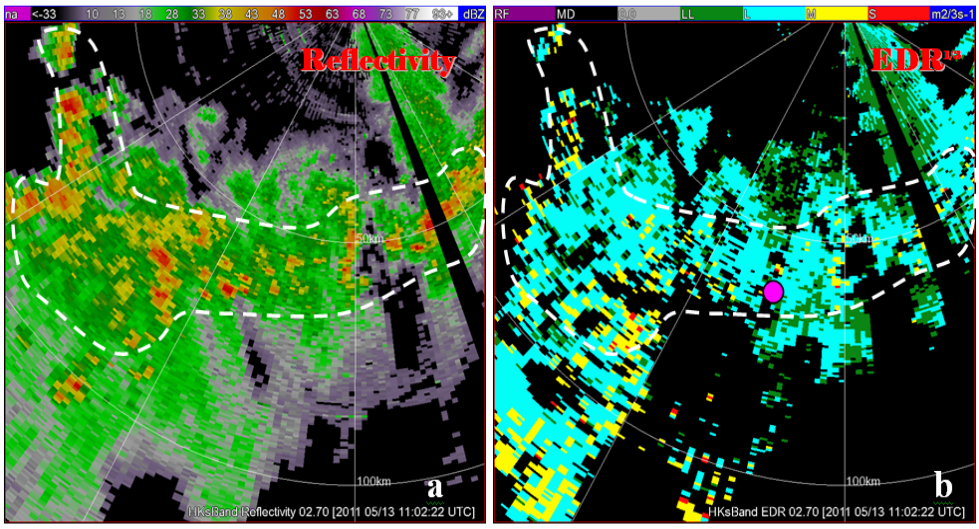

Fig. 10(c). Reflectivity (left) and $EDR^{1/3}$ (right) fields at elevation angle of 2.7° at 11:02 UTC on 23 May, 2011. Purple dot marks the location where aircraft $EDR^{1/3}$ is 0.41 $m^2/3s^{-1}$. The colour scale of right hand side is the same as that of Fig. 5(a) (ii)

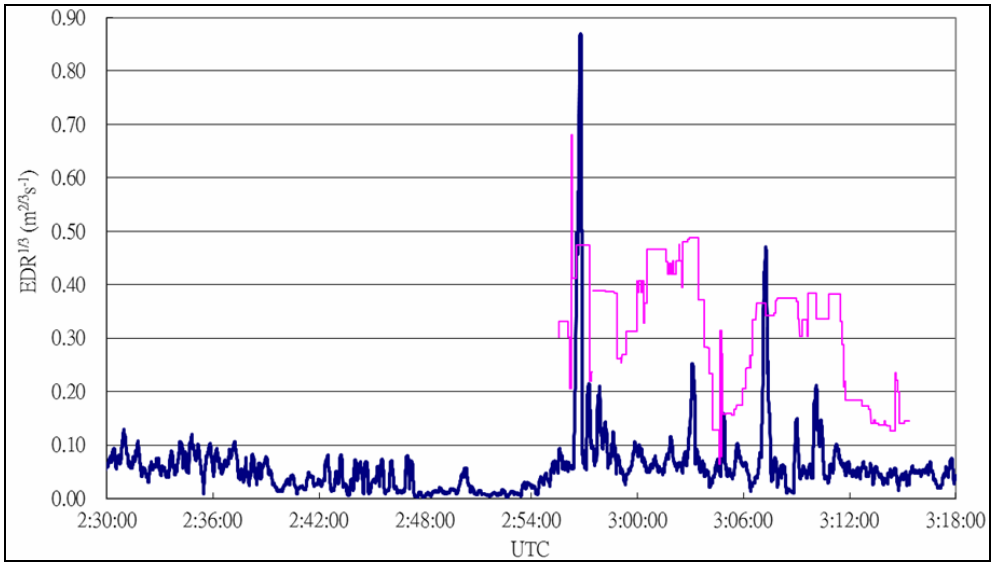

Fig. 10(d). Time series graph for comparing $EDR^{1/3}$ between aircraft (blue) and radar (pink). Comparison of $EDR^{1/3}$ between aircraft and radar for the second turbulence case

meteorological information to the cockpit is being planned. The EFB allows processing of the data from the flight management system (FMS) of the aircraft, so that EDR could be calculated and displayed in realtime. This would provide additional information about the turbulence experienced by the aircraft. The pilot could make reference to the radar onboard the aircraft to avoid areas of high turbulence. But the present product based on long-range radar has the advantage that it covers a larger area so that the pilot could have better view about the turbulence distribution.

For more detailed comparison between radar-based and aircraft-based EDR, the radar-based EDR along the flight route is extracted. This is extracted in such a way that: (i) only the EDR values within 8 km from the flight route is considered and (ii) for all those values considered, only the maximum value of $EDR^{1/3}$ is extracted. The

$EDR^{1/3}$ value extracted in this way is called radar-based $EDR^{1/3}$ for simplicity. The radar-based and aircraft-based $EDR^{1/3}$ values near the time of the encounter of moderate to severe turbulence are shown in Fig. 5(b). It could be seen that the two values generally vary in phase, though the maximum value of $EDR^{1/3}$ for the event is different from the two datasets. Nonetheless, the radar-based $EDR^{1/3}$ value could provide helpful advance advice to the pilot about the severity of the turbulence to be encountered.

4. Second example – Severe turbulence on 13 May, 2011

According to the news report, an aircraft flying from Beijing to Hong Kong encountered severe turbulence when it was about 15 minutes to land at HKIA. Seat belt sign was on and most passengers were seated with the seat belts fastened. However, seven persons on the aircraft were still injured, including 2 passengers and 5 crew members.

Based on the aircraft data, the peak of the turbulence event occurred at about 02:56:43 UTC, 13 May, 2011. At that time, the aircraft was descending at about 6,000 m above sea level on the way to HKIA [Fig. 6(a)]. The vertical acceleration [Fig. 6(b)] also fluctuated rapidly. At about 02:56 UTC, it varied between +1.9 and -0.5 g. However, based on the flight altitude recorded onboard the aircraft [Fig. 6(a)], there were not much change in the altitude of the aircraft as a result of the turbulence encounter. May be the turbulence encounter in this case is rather brief.

It turns out that the wind was not very strong at the time of the event. From Fig. 7(a), the wind speed had a maximum value of 11 m/s only around that time. The wind direction fluctuated quite a lot, from Fig. 7(b), with mainly northerly winds at the event time. Synoptically, a surface trough of low pressure affected the south China coastal areas. It just moved southwards and passed the coast at 0000 UTC, 13 May, with the weak northerly winds associated with a continental high centre affecting the coast. Return flow (southerly winds) could be identified at 850 hPa. West to northwesterly winds with short waves affected the southern China in the middle troposphere. The surface trough, return flow at lower troposphere and short westerly waves in the middle troposphere all contributed towards the occurrence of convective weather near Hong Kong.

To examine the effect of the weather on the operation of the aircraft, the time series of $EDR^{1/3}$ and F-factor are plotted in Figs. 8(a&b) respectively. It could be seen that, at the climax of the event, the $EDR^{1/3}$ reached a maximum value of 0.86 $m^{2/3}s^{-1}$. The event is clearly associated with severe turbulence, following the definition of ICAO (2010) for en-route aircraft. In the period of 02:56 to 02:57 UTC, the F-factor also got to the rather high value of +0.5 to -0.54. The event could thus adversely affect the operation of the aircraft in terms of turbulence and wind shear.

The $EDR^{1/3}$ value obtained from the flight data is plotted along the flight route, which in turn is overlaid on the radar imagery of reflectivity at a height of 6000 m above sea level in Fig. 9(a). It could be seen that the severe turbulence appears to be associated with a small but rather intense rain cell, with an estimated rainfall rate in the region of 30 to 50 mm/hour. At that location of the event, the spectrum width of the radar is also rather large, reaching about 3 m/s [Fig. 9(b)]. The Doppler velocity seems to reach 10 m/s or so in association with the rain cell [Fig. 9(c)].

The $EDR^{1/3}$ derived from the radar's spectrum width is also compared with the aircraft measurement. At the climax of the event [Fig. 10(a)], the former is found to reach about 0.68 $m^{2/3}s^{-1}$ inside the rain cell. Though this value is a bit small compared with the maximum $EDR^{1/3}$ value from the aircraft data, it nonetheless could hint the pilot that there could be a chance of severe turbulence (close to 0.7 $m^{2/3}s^{-1}$) in association with the rather small, isolated rain cell. If such radar-based $EDR^{1/3}$ data could be uplinked to the aircraft in real time, the pilot may choose not to fly into the cell but go around it.

In order to see that the radar-based $EDR^{1/3}$ is not causing false alarms about the occurrence of severe turbulence, its values at other times of the flight are also considered in Figs. 10(b&c), when the aircraft-based $EDR^{1/3}$ values are much smaller than that at the climax of the turbulence event. It could be seen from these figures that the radar-based $EDR^{1/3}$ is generally consistent with the aircraft value.

Once again, the radar-based and aircraft-based $EDR^{1/3}$ values are compared in Fig. 10(d). The radar-based $EDR^{1/3}$ value is extracted within 5 km from the flight path, and the maximum value with the 5-km tube from the flight path is considered. It could be seen that the two datasets in general vary in phase, though the magnitude of $EDR^{1/3}$ value could be different. Nonetheless, the radar-based $EDR^{1/3}$ value could provide helpful advance advice to the pilot about the severity of the turbulence to be encountered. In the absence of fool proof onboard turbulence alert products available, alerts using ground based observations shall be attempted and communicated to the pilots onboard on trial mode which will be of prophylactic value. However, operationalising

these products shall be done only on getting feedback from the pilots.

5. Conclusions

The spectrum width data for a S-band radar at Hong Kong are used to calculate EDR by removing the wind shear contribution. The EDR maps so obtained from the conical scans of the radar are used to compare with the aircraft-measured turbulence intensity in two cases of moderate to severe turbulence occurring around Hong Kong. In that two cases under study, the wind data measured onboard the aircraft are used to calculate EDR and F-factor, which show that the wind disturbances have significant impact on the operation of the aircraft. The disturbed airflow appears to be associated with intense, through rather small and isolated, rain cell as shown on the radar reflectivity imagery. The spectrum width at the location of the rain cell is also quite large, of the order of 3 to 4 m/s. The EDR values determined from the spectrum width data are generally consistent with the aircraft measurements. If the EDR maps could be uplinked to the cockpit, the pilot may not choose to go through the rain cells but possibly fly around them. Due to busy air traffic and limited air space, the aircraft may need to fly close to the convective clouds. As such, apart from the onboard radar data, the data collected by long-range, ground-based radars would be useful to the pilots as well if foolproof communication is established to disseminate the ground based data to the pilot onboard.

The spectrum width data from a S-band radar appear to have potential of generating turbulence intensity mosaic in the vicinity of Hong Kong for alerting the en-route aircraft about the chance of occurrence of severe turbulence. More cases of moderate to severe turbulence would be considered in future studies, and the radar-based EDR values would be compared with the aircraft measurements if the latter are available. This comprehensive study would be used to establish the quality of the radar-based EDR for turbulence alerting service. Similar turbulence detection algorithm may also be applied to the other long-range radars in the Pearl River Delta region in order to extend the coverage of the turbulence intensity mosaic.

Acknowledgements

Constructive comments of the unanimous referee to improve the quality of the paper is acknowledged.

References

Brewster, K. A. and Zrnic, D. S., 1986, "Comparison of eddy dissipation rate from spatial spectra of Doppler velocities and Doppler spectrum widths", *J. Atmos. Oceanic Technol.*, **3**, 440-452.

Chan, P. W., 2011, "Generation of an eddy dissipation rate map at the Hong Kong International Airport based on Doppler Lidar data", *Journal of Atmospheric and Oceanic Technology*, **28**, 37-49.

Chan, P. W., 2009, "Atmospheric turbulence in complex terrain: verifying numerical model results with observations by remote-sensing instruments", *Meteorology and Atmospheric Physics*, **103**, 145-157.

Clark, T. L., Keller, T., Coen, J., Neilley, P., Hsu, H. and Hall, W. D., 1997, "Terrain-induced turbulence over Lantau Island: 7 June 1994 Tropical Storm Russ case study", *J. Atmos. Sci*., **54**, 1795-1814.

Cornman, L. B., Meymaris, G. and Limber, M., 2004, "An update on the FAA Aviation Weather Research Program's in situ turbulence measurement and reporting system", Preprints, Eleventh Conf. on Aviation, Range and Aerospace Meteorology, Hyannis, MA, *Amer. Meteor. Soc*., p4.3.

Doviak, R. and Zrnic, D., 2006, "Doppler Radar and Weather Observations", 2nd edition, Dover Publications, p592.

Fang, M., Doviak, R. J. and Melnikov, 2004, "Spectrum width measured by the WSR-88D radar: Error sources and statistics of various weather phenomena", *J. Atmos. Oceanic Technol.*, **21**, 888-904.

Gilbert, D., Cornman, L. B., Rodi, A. R., Frechlich, R. G. and Goodrich, R. K., 2004, "Calculating EDR from aircraft wind data during flight in and out of Juneau AK: Techniques and challenges associated with non-straight and level flight patterns", Preprints, 11th Conf. on Aviation, Range and Aerospace Meteorology. Hyannis, MA, *Amer. Meteor. Soc*., CD-ROM, 4.4.

Haverdings, H. and Chan, P. W., 2010, "Quick Access Recorder (QAR) data analysis software for windshear and turbulence studies", *Journal of Aircraft*, **47**, 4, 1443-1447, July-August 2010.

Hinton, D. A., 1993, "Airborne Derivation of Microburst Alerts from Ground-based Terminal Doppler Weather Radar Information – A Flight Evaluation", NASA Technical Memo. 108990, p32.

International Civil Aviation Organization (ICAO), 2010, "Meteorological service for international air navigation", Annex 3 to the convention on international civil aviation, 17th edition, July 2010, p206.

Labitt, M., 1981, "Coordinated radar and aircraft observations of turbulence", Project Rep. ATC 108, MIT, Lincoln Lab, p39.

Merritt, M. W., 1987, "Automated detection of microburst windshear for Terminal Doppler Weather Radar, presented at SPIE Conference on Digital Image Processing and Visual Communications Technologies in Meteorology", 27-28 October, 1987, Cambridge, MA, USA.

Proctor, F. H., Hinton, D. A. and Bowles, R. L., 2000, "A wind shear hazard index, presented at 9th Conference on Aviation, Range and Aerospace Meteorology", 11-15 September, 2000, Orlando, FL., USA.

Shun C. M. and Chan, P. W., 2008, "Applications of an infrared Doppler Lidar in detection of wind shear", *Journal of Atmospheric and Oceanic Technology*, **25**, 637-655.

Williams, J. K., Cornman, L. B., Yee, J., Carson, S. G., Blackburn, G. and Craig, J., 2006, "NEXRAD detection of hazardous turbulence", 44th AIAA aerospace sciences meeting and exhibit, Reno, Nevada, USA, AIAA 2006-0076.

Zhang, P., Chan, P. W., Doviak, R. and Fang, M., 2009, "Estimate of eddy dissipation rate using spectrum width observed by the Hong Kong TDWR radar", 34th Conference on Radar Meteorology, American Meteorological Society, Williamsburg, VA, USA, 5-9 October, 2009.